Volume 52
Number 47
21 December 2023
Pages 17585-18104

Dalton Transactions

An international journal of inorganic chemistry

rsc.li/dalton

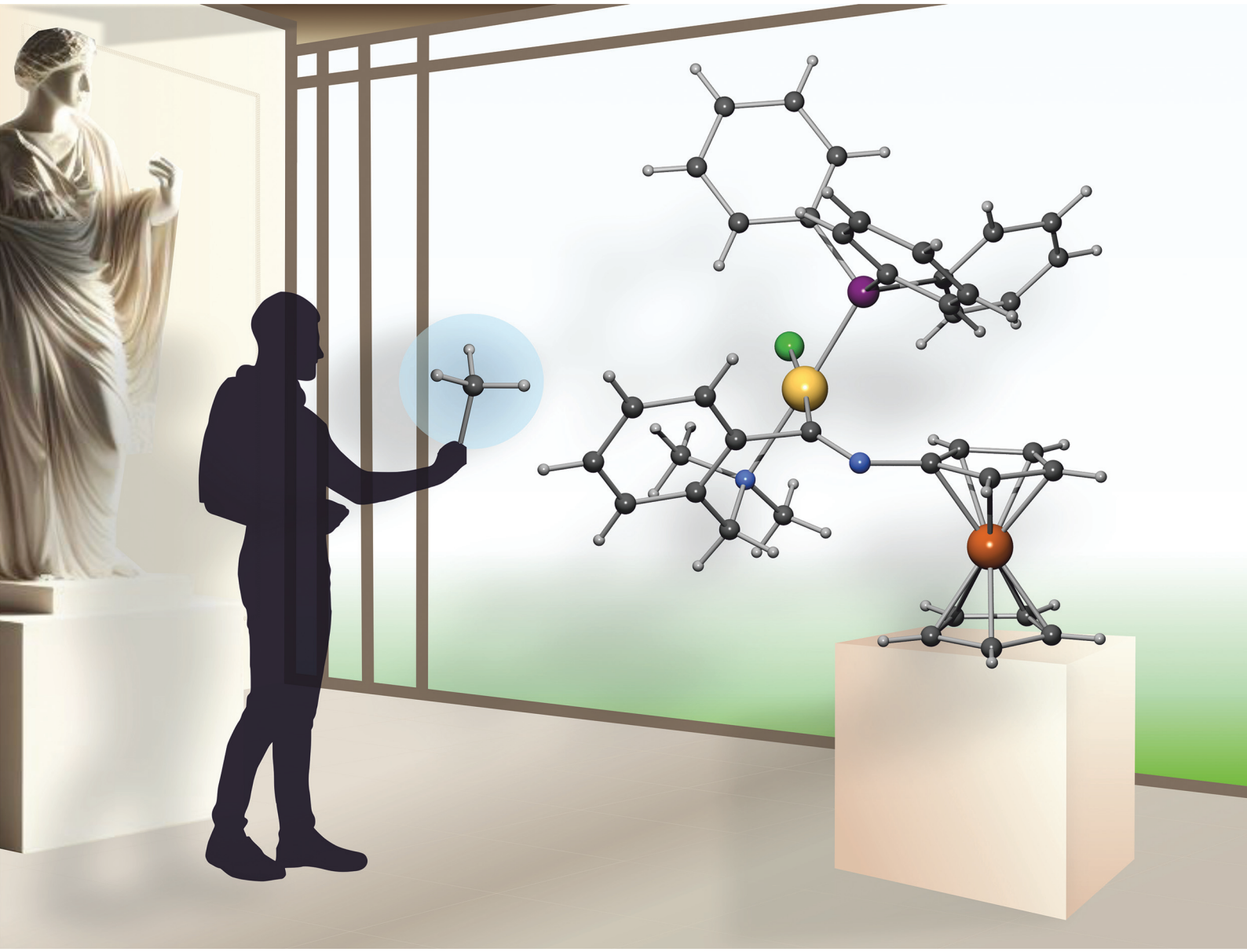

ISSN 1477-9226

ROYAL SOCIETY OF CHEMISTRY

PAPER

Petr Štěpnička *et al.*

Synthesis and reactivity of Pd(II) imidoyl complexes obtained by insertion of isocyanoferrocene into the Pd–C bonds of orthopalladated precursors

Dalton Transactions

ROYAL SOCIETY OF CHEMISTRY

PAPER

View Article Online
View Journal | View Issue

Check for updates

Cite this: *Dalton Trans.*, 2023, **52**, 17701

Synthesis and reactivity of Pd(II) imidoyl complexes obtained by insertion of isocyanoferrocene into the Pd–C bonds of orthopalladated precursors†

Michal Franc, Petr Vosáhlo, Jiří Schulz, Ivana Císařová and Petr Štěpnička *

While the multifaceted reactivity of organic isocyanides has been extensively demonstrated, that of their organometallic analogue, isocyanoferrocene (FcNC; Fc = ferrocenyl), has not yet been adequately explored. This contribution describes the syntheses of novel chelating Pd(II) imidoyl complexes, [(YCH$_2$C$_6$H$_4$C(NFc)-κ^2*Y*,*C*)PdCl(PR$_3$)], by insertion of FcNC into the Pd–C bond of cyclopalladated precursors [(YCH$_2$C$_6$H$_4$-κ^2*Y*,*C*)PdCl(PR$_3$)] (Y = Me$_2$N, MeS, R = Ph, Me). The imidoyl complexes underwent facile alkylation with [Me$_3$O][BF$_4$] to produce the cationic aminocarbene complexes [{YCH$_2$C$_6$H$_4$C(N(Me)Fc)-κ^2*Y*,*C*}PdCl(PR$_3$)][BF$_4$]. All compounds were fully characterised using a combination of spectroscopic methods (NMR, FTIR and ESI MS), cyclic voltammetry and single-crystal X-ray crystallography. In addition, DFT calculations were used to describe the bonding in the two compound families. Analyses with intrinsic bond orbitals (IBOs) and the quantum theory of atoms in molecules (QTAIM) consistently pointed to the transformation of an X-type imidoyl C-ligand (σ-organyl) into an L-type carbene donor upon alkylation, which has only a minor structural consequence. Also reported is the unexpected conversion of the imidoyl complex [(Me$_2$NCH$_2$C$_6$H$_4$C(NFc)-κ^2*N*,*C*)PdCl(PPh$_3$)] into (*Z*)-2,2-dimethyl-1-(ferrocenylimino)isoindolin-2-ium tetrafluoroborate as a reductive elimination product, which was induced by Lewis and Brønsted acids.

Received 21st August 2023,
Accepted 5th October 2023

DOI: 10.1039/d3dt02717a

rsc.li/dalton

Introduction

Specific electron properties including partial carbene character[1] endow isocyanides with unique reactivity[2] and the ability to coordinate transition metals. In addition to being specific σ-donor and π-acceptor ligands,[3] coordinated isocyanides readily add alcohols and amines to produce heteroatom-stabilised carbene complexes (reaction **A** in Scheme 1)[4,5] and insert into metal–carbon bonds to afford imidoyl complexes that can be further transformed into aminocarbene complexes by protonation or alkylation (reaction **B** in Scheme 1).[6]

We have shown that **A** and **B**-type reactions of 1′-(diphenylphosphino)-1-isocyanoferrocene[7] afford structurally unique P-chelated aminocarbene complexes (Scheme 2).[8] Now, we focus on similar reactions of isocyanoferrocene (FcNC, Fc = fer-

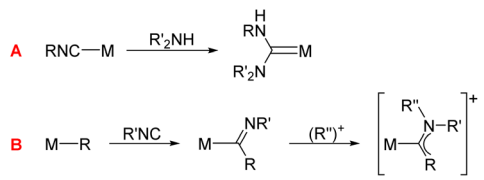

Scheme 1 Reactions of isocyanides relevant to this work.

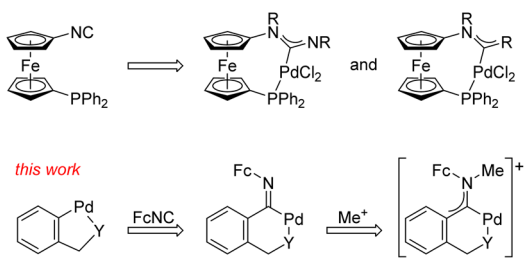

Scheme 2 Examples of P-chelated Pd(II) carbene complexes accessible from 1′-(diphenylphosphino)-1-isocyanoferrocene and the aims of the present work focused on isocyanoferrocene (FcNC; Fc = ferrocenyl, Y = NMe$_2$ or SMe).

Department of Inorganic Chemistry, Faculty of Science, Charles University, Hlavova 2030, 128 40 Prague, Czech Republic. E-mail: stepnic@natur.cuni.cz

†Electronic supplementary information (ESI) available: Complete experimental procedures and characterisation data, summary of crystallographic parameters, additional structure diagrams and cyclic voltammograms, results from IBO analysis, and copies of the NMR spectra. CCDC 2288861–2288870. For ESI and crystallographic data in CIF or other electronic format see DOI: https://doi.org/10.1039/d3dt02717a

rocenyl) with cyclometallated Pd(II) precursors. While isocyanide insertions into Pd–C bonds in complexes with orthopalladated ligands are well documented,[9,10] subsequent transformations of the resulting imidoyl complexes into carbenes have seldom been reported.[6]

In this contribution, we describe our study of the reactions between FcNC[11,12] and Pd(II) complexes containing orthopalladated benzylamine and benzyl thioether ligands that produced chelating imidoyl complexes, which were subsequently converted into ferrocene-substituted[13] Fischer-type aminocarbene complexes with redox-active ferrocenyl pendants by alkylation (Scheme 2, bottom). In particular, we report the syntheses of two series of Pd(II) complexes (imidoyl and aminocarbene) and detailed structural characterisation using a combination of spectroscopic methods, X-ray diffraction analysis, cyclic voltammetry, and DFT calculations. The results of reactivity studies on the imidoyl complexes, which led to the isolation of a structurally uncommon, reductive elimination product, are also reported.

Results and discussion

Syntheses and structural characterisation

The orthopalladated complexes **1** and **2** were synthesised by cleavage of the respective dimeric precursors $[(L^{CY})PdCl]_2$ with trimethylphosphine and triphenylphosphine (Scheme 3). The reactions with the more stable and easier-to-dose PPh_3 were performed using stoichiometric amounts of the starting materials and afforded pure **1a** and **2a** in practically quantitative yields. The analogous reactions with PMe_3 required a slight excess of this air-sensitive phosphine to avoid incomplete conversion of the dimeric Pd(II) precursors. While cleavage of the "benzylamine" complex $[(L^{CN})PdCl]_2$ (L^{CN} = 2-$Me_2NCH_2C_6H_4$-κ^2N,C^1) proceeded selectively and produced pure **1b** in virtually quantitative yield after simple chromatographic purification, the reaction with the thioether analogue, $[(L^{CS})PdCl]_2$ (L^{CS} = 2-$MeSCH_2C_6H_4$-κ^2S,C^1), gave **2b** contaminated with the bisphosphine complex *trans*-[(2-$MeSCH_2C_6H_4$-κC^1)$PdCl(PMe_3)_2$] (*trans*-**3**), arising *via* decomplexation of the thioether arm by excess PMe_3.[14] The unwanted formation of *trans*-**3** was suppressed by lowering the amount of PMe_3 to a strictly stoichiometric amount (Pd : PMe_3 = 1 : 1). Conversely, increasing the amount of PMe_3 to 2 equiv. per Pd resulted in the selective formation of *trans*-**3**, which was isolated and fully characterised, including structure determination (see ESI, Fig. S1†).

In the next step, compounds **1** and **2** were treated with isocyanoferrocene (1 equiv.) in dichloromethane to produce the respective imidoyl complexes **4** and **5** (Scheme 3). Subsequent methylation with the Meerwein salt, $[Me_3O][BF_4]$, in CH_2Cl_2 converted these insertion products into the cationic aminocarbene complexes **6** and **7**. Both the imidoyl and carbene complexes were purified by column chromatography over silica gel and isolated in generally good yields (75–90%).

Imidoyl complexes **4** and **5** displayed ions due to $[M - Cl]^+$ in the ESI MS spectra. Their ^1H and ^{13}C NMR spectra showed four separate signals for the CH groups of the ferrocene C_5H_4 ring, which suggested fixed conformation that rendered these groups diastereotopic (at room temperature). The L^{CS} complexes were inherently chiral due to the presence of a stereogenic sulfur atom, which itself made the protons at the ferrocene C_5H_4 ring diastereotopic. One of the C_5H_4 signals in the ^1H NMR spectrum was always observed at a markedly lower field (δ_H 6.1–6.4) than the remaining three signals, very likely due to shielding anisotropy. The diastereotopic methyl groups (only for L^{CN}) and methylene protons also gave rise to separate signals. The $^3J_{PC}$ and $^4J_{PH}$ coupling constants observed for the CH_2NMe_2 groups in **4a** and **4b** were consistent with the *trans*-P,N arrangement; the resonances due to the CH_2SMe arms were typically observed as broad signals.

The ^{13}C NMR signals of the Pd-bound imidoyl carbons in **4** and **5** were observed near 190 ppm (d, J_{PC} = 2–3 Hz), and the spectra also showed characteristic, low-field signals for the ferrocene C^{ipso}–N carbons, which were split into doublets *via* interactions with phosphorus (δ_P 104–106, J_{PC} = 4–6 Hz; *cf.* δ_C 105.6 for $FcNH_2$ [15]). The ^{31}P NMR signals of **4** and **5** were detected upfield of those for **1** and **2**. However, the magnitude of the shift was considerably larger for the triphenylphosphine complexes (Δ_P = −16.5 and −13.5 ppm for **4a** and **5a**, respectively) than for their PMe_3 analogues (Δ_P = −1.3 ppm for **4b**, and −1.4 ppm for **5b**). The IR bands attributable to the C=N stretching modes were observed at approximately 1600 cm^{-1}.

Methylation of the imidoyl complex to give Fischer carbenes **6** and **7** altered the NMR spectra rather marginally. The salient change was a downfield shift of the ^{13}C NMR signal due to the Pd-bound carbon atom, as is typical for carbene complexes (δ_C 227–230 ppm), and the appearance of additional signals due to the introduced methyl group ($\delta_H \approx 3.4$–4.0, $\delta_C \approx 48$). The presence of the BF_4^- anion was corroborated by intense and structured ν_3 bands at approximately 1060 cm^{-1} in the IR spectra.[16] Consistent with their ionic nature, the carbene complexes displayed strong peaks due to $[M - BF_4]^+$ in their ESI

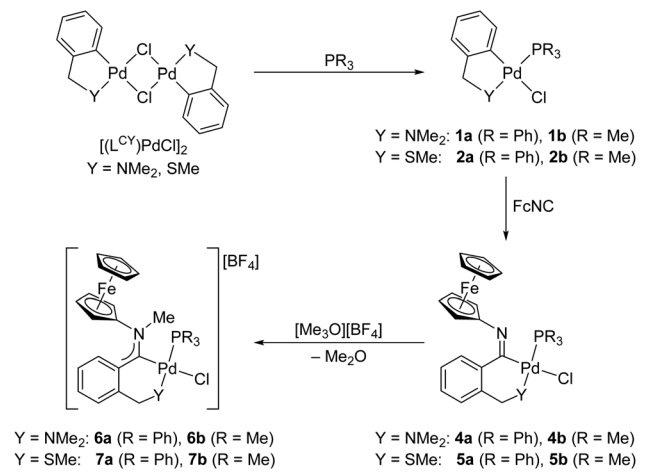

Scheme 3 Syntheses of imidoyl complexes **4** and **5** and their subsequent conversion into carbene complexes **6** and **7** by methylation (all reactions were performed in dichloromethane).

MS. Another notable feature was a colour change from orange to red noted visually during the synthesis and illustrated by UV-vis measurements for the pair of compounds **4b** and **6b** (Fig. 1). In the visible region, imidoyl complex **4b** displayed an absorption band at 449 nm (ε = 710 M^{-1} cm^{-1} in CH_2Cl_2), which was bathochromically shifted with respect to that of ferrocene itself (440 nm in ethanol)[17] due to the extended conjugated system. After alkylation to give **6b**, the absorption band shifted further to lower energies (485 nm), and its intensity increased (ε = 1555 M^{-1} cm^{-1}).

The structures of all imidoyl and carbene complexes were determined by single-crystal X-ray diffraction analysis. The structures of the representative imidoyl complexes **4a** and **5b** are shown in Fig. 2 (complete structure diagrams are available in the ESI†). Selected geometric parameters are summarised in Table 1. All compounds crystallised with one structurally independent molecule except for **4b**·0.35H_2O, which contained two almost identical complex molecules in the asymmetric unit and a water molecule with partial occupation.

In all imidoyl complexes, the coordination sphere of the Pd atom was essentially planar, and the interligand angles did not depart significantly from 90°. The Pd-donor distances were unexceptional and varied only slightly over the entire series, except for the Pd–Y bonds. Notably, the influence of the Y atom on the Pd–P bond in the *trans* position was also small (the Pd–P bond was approximately 0.02 Å longer in **5a**/**5b** than in **4a**/**4b** due to the larger *trans* influence[18] of the S-donor group). In addition, the Pd–PPh_3 bonds were somewhat longer than the Pd–PMe_3 bonds for steric reasons.

The Pd–C (≈1.97–1.99 Å) and C1–N1 (≈1.27 Å) bond lengths in **4** and **5** were similar to those reported for [Pd{C(R^1)═NR^2}Cl(PR_3)$_2$] (R^1 = 2-pyridyl, R^2 = 4-MeOC_6H_4, PR_3 = PMe_2Ph;[19] R^1 = Me, R^2 = 2,6-$Me_2C_6H_3$, (PR_3)$_2$ = dppe;[20] and R^1 = Me, R^2 = 2-vinylphenyl, PR_3 = PEt_3[21]) and for the chelate compounds obtained from 1′-(diphenylphosphino)-1-isocyanoferrocene,[7] while the C1–N1 bond lengths did not differ much from those of ferrocene imines FcCH═NAr (Ar = aryl).[22] The arrangements at the C1═N1 bonds were *anti* (torsion angles C2–C1–N1–C11 are 176–179°) and the attached ferrocene units were rotated by 21–25° with respect to the {N1,C1,C2} plane (the range of the dihedral angles between the C(11–15) ring and the carbene plane is given), thereby maintaining conju-

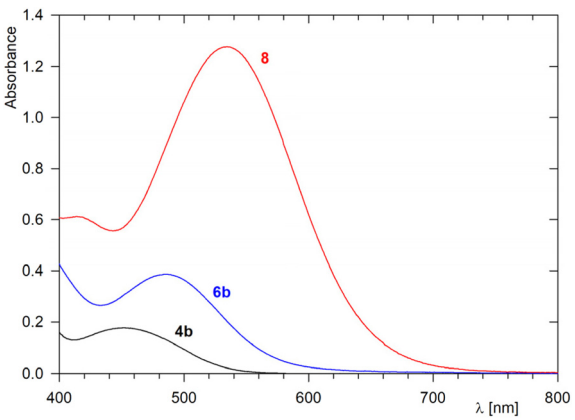

Fig. 1 UV-vis spectra of **4b**, **6b** and **8** (*c* = 0.50 mM in CH_2Cl_2; optical path: 1 cm).

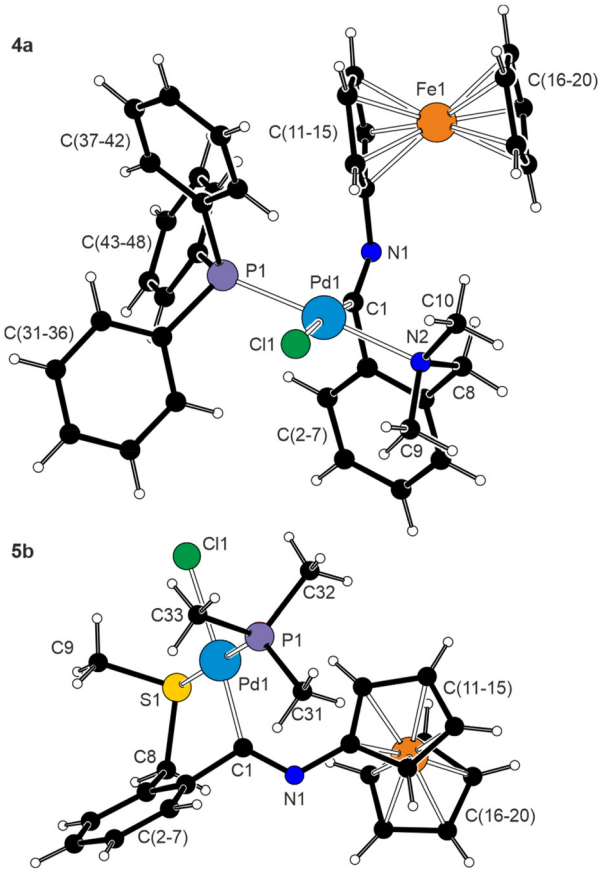

Fig. 2 Molecular structures of **4a** and **5b** (for displacement ellipsoid plots and additional structure diagrams, see the ESI†).

Table 1 Selected distances and angles for imidoyl complexes **4** and **5** (in Å and deg)

Parameter	**4a**	**4b**·0.35H_2O[b]	**5a**[c]	**5b**
Y	N2	N2/N4	S1	S1
Pd1–C1	1.986(3)	1.979(2)/1.972(2)	1.994(1)	1.994(3)
Pd1–Y	2.201(2)	2.210(1)/2.202(1)	2.386(2)	2.3858(7)
Pd1–P1	2.2657(8)	2.2513(5)/2.2495(5)	2.2916(6)	2.2705(7)
Pd1–Cl1	2.4156(7)	2.4122(5)/2.4156(6)	2.4091(5)	2.4115(7)
C1–Pd1–Y	85.64(9)	87.46(6)/87.26(6)	86.80(7)	88.34(7)
C1–Pd1–P1	94.39(7)	92.16(5)/90.60(5)	94.58(4)	90.87(7)
Cl1–Pd1–Y	89.51(6)	92.50(4)/93.45(4)	85.80(7)	90.84(2)
Cl1–Pd1–P1	90.39(3)	87.88(2)/88.82(2)	92.77(2)	89.87(2)
C1–N1	1.265(3)	1.274(2)/1.278(2)	1.271(2)	1.272(3)
N1–C11	1.410(4)	1.412(2)/1.409(2)	1.404(2)	1.409(3)
N1–C1–C2	117.6(2)	118.4(1)/119.2(1)	117.6(1)	119.0(2)
C1–N1–C11	123.3(2)	122.7(1)/122.1(1)	123.7(1)	122.1(2)
φ[a]	−176.2(2)	176.3(1)/−177.3(1)	−178.5(1)	179.3(2)

[a] φ is the torsion angle C11–N1–C1–C2; C2 is the pivotal carbon atom from the C(2-7) phenyl ring bonding to C1. [b] Data for molecule 1/molecule 2. [c] The Pd-bound SMe group was disordered and was refined over two positions; parameters for the dominant orientation are given.

gation.[23] The ferrocene moieties adopted their usual geometries with similar Fe–C distances and negligible tilt angles (<3°). Finally, the C_6H_4 ring attached to the carbene C1 atom was twisted by approximately 70° from the plane defined by the palladium and its four ligating atoms and by 71–89° from the "imidoyl" {N1,C1,C2} plane.

The structures of aminocarbene complexes **6a**·$CHCl_3$ and **7a** are displayed in Fig. 3 (for additional structure plots, see the ESI†). Inspection of the data outlined in Table 2 and comparison with those of **4** and **5** revealed that *N*-methylation to give aminocarbene complexes affected the coordination sphere of Pd(II) only marginally. Compared to the respective imidoyl precursors, the carbene complexes showed shorter Pd–Cl bonds (by 0.05–0.06 Å), presumably due to the decreased *trans* influence,[24] and slightly shorter Pd–C distances (0.01–0.03 Å) due to increased Pd–C bond orders. Correspondingly, the N1–C1 bond was longer (≈0.03 Å), which suggested partial loss of the double bond (imine) character; similar elongation was observed for the N1–C11 bond. The presence of a third substituent at the N atom resulted in opening of the N1–C1–C2 angle to 120°, while the C1–N1–C11 angle remained almost unchanged. Individual parameters compared well with the values reported for similar compounds featuring cyclic pyridine-2-ylidene ligands.[25]

Table 2 Selected distances and angles for imidoyl complexes **6** and **7** (in Å and deg)

Parameter	**6a**·$CHCl_3$	**6b**	**7a**	**7b**[b]
Y	N2	N2	S1	S1
Pd1–C1	1.978(2)	1.954(2)	1.973(3)	1.960(3)
Pd1–Y	2.187(2)	2.211(2)	2.365(1)	2.395(1)
Pd1–P1	2.2725(8)	2.2606(5)	2.301(1)	2.273(1)
Pd1–Cl1	2.3635(7)	2.3590(5)	2.3547(9)	2.350(1)
C1–Pd1–Y	86.8(1)	86.92(7)	87.2(1)	86.3(1)
C1–Pd1–P1	93.85(8)	92.34(6)	93.8(1)	93.3(1)
Cl1–Pd1–Y	91.77(6)	92.40(4)	87.48(4)	90.81(4)
Cl1–Pd1–P1	87.60(3)	88.32(2)	91.53(4)	89.90(4)
C1–N1	1.298(4)	1.305(2)	1.301(4)	1.304(5)
N1–C11	1.431(4)	1.436(2)	1.431(4)	1.440(5)
N1–C21	1.491(3)	1.487(3)	1.533(4)	1.512(6)
N1–C1–C2	120.1(2)	120.8(2)	119.4(3)	120.1(3)
C1–N1–C11	123.6(2)	122.8(2)	123.1(3)	123.3(3)
φ[a]	170.4(2)	177.5(2)	−177.6(3)	177.1(3)

[a] φ is the torsion angle C11–N1–C1–C2; C2 is the pivotal carbon atom from the C(2-2) phenyl ring bonding to C1. [b] The Pd-bound SMe group was disordered and was refined over two positions; parameters for the dominant orientation are given.

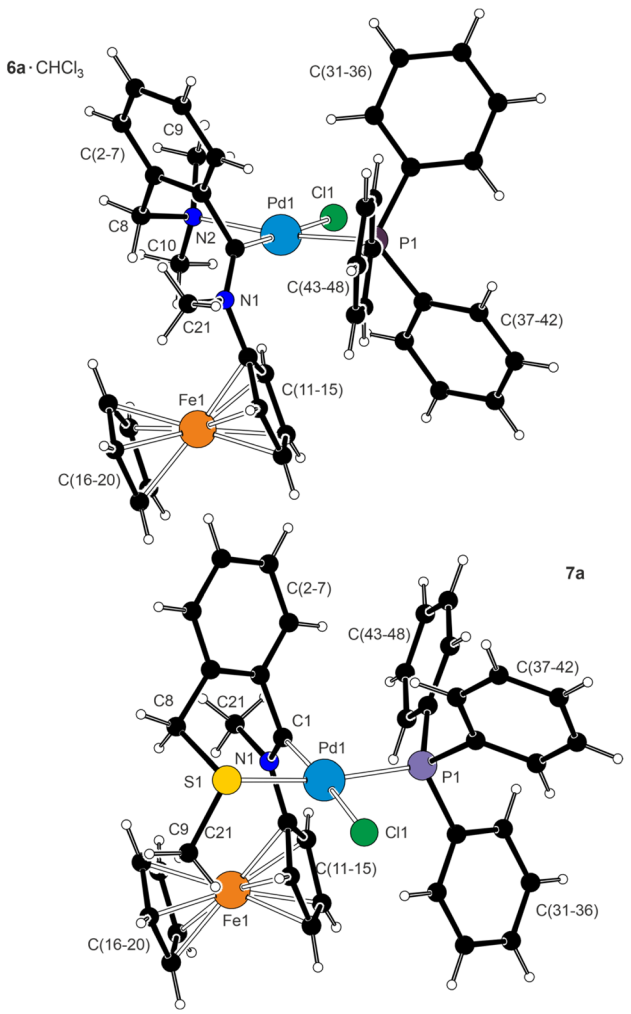

Fig. 3 Molecular structures of **6a**·$CHCl_3$ and **7a** (for displacement ellipsoid plot and additional structural diagrams, see the ESI†). The counter ions ($[BF_4]^-$) and the solvent molecule were omitted for clarity.

Even in **6** and **7**, the phenylene rings were twisted with respect to the coordination plane (by 64–73°) and to the carbene moiety {N1,C1,C2} (by 75–84°). The ferrocene units remained virtually unperturbed (with tilt angles less than ≈3.5°), and their C(11–15) rings were rotated by 26.0(4)° (in **7b**) to 38.5(4)° (in **7a**) from the {N1,C1,C2} planes.

Description of the bonding situation

The similarity of the molecular structures led us to examine the bonding situations in the imidoyl and carbene complexes using theoretical methods and compounds **4a** and **6a** as the representative pair. An analysis using the intrinsic bond orbital (IBO)[26] approach has already revealed different electron sharing between the individual donor atoms and the Pd(II) centers. Specifically, the IBOs corresponding to the coordination bonds between palladium and the hard donors (N and Cl) in complex **4a** showed greater charge localisation on the donor atoms [N(1.70)/Pd(0.17), Cl(1.76)/Pd(0.16)], which was consistent with their lower polarizabilities and indicated higher ionicity of the Pd–N and Pd–Cl dative bonds. As such, these bonds are more easily deformed, which was reflected by the relatively larger differences between the calculated and experimental bond distances. Conversely, electron sharing between the soft phosphine and imidoyl ligands and Pd(II) was considerably larger and increased from the phosphine [P(1.49)/Pd(0.42)] to the imidoyl [C(1.15)/Pd(0.81)] moiety, suggesting more covalent bonding in the latter case (Fig. 4). The IBO analysis also indicated negligible π-backbonding from Pd to the phosphorus and the imidoyl carbon and exposed the

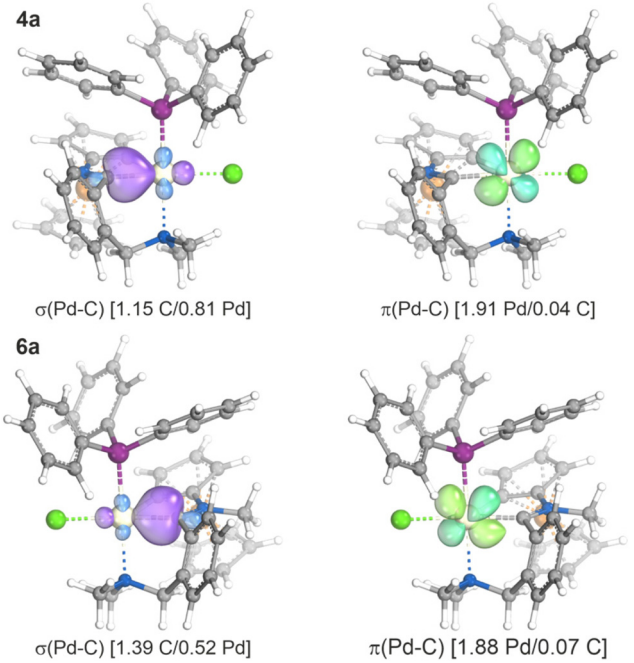

Fig. 4 Intrinsic bond orbitals relevant to the Pd–C bonds in **4a** and **6a** (values in parentheses indicate the fraction of σ and π bonding electrons assigned to the individual atoms). For additional diagrams, see ESI.†

presence of a lone electron pair on the imidoyl nitrogen (*vide infra*).

Carbene formation by methylation of the imidoyl moiety was accompanied by a change from an X-type Pd–C interaction in **4a** (σ-bonded imidoyl carbon) to an L-type interaction[27] in **6a** [C(1.39)/Pd(0.52); donation of the carbene lone pair]. Notably, the altered nature of the Pd–C bond also affected the other Pd-donor interactions. This influence was particularly evident for the *trans*-chloride [Cl(1.67)/Pd(0.26)] and *cis*-PPh_3 ligands [P(1.39)/Pd(0.55)], while the NMe_2 moiety was less affected [N(1.68)/Pd(0.19)].

Subsequent topological analysis of the calculated electron density using Bader's Quantum theory of atoms in molecules (QTAIM)[28] supported the results obtained with the IBO approach. Low electron densities (ρ_{bcp}) and positive values for the electron density Laplacians ($\nabla^2\rho_{bcp}$) at the bond critical points (bcp) between palladium and the coordinated atoms in both model complexes (Table 3) pointed to closed-shell interactions (either ionic, dative, or van der Waals), in this case a donor–acceptor bond involving a heavy metal element.[29] The potential-to-kinetic energy density ratios ($|V_{bcp}|/G_{bcp}$) fell into the intermediate region ($2 > |V_{bcp}|/G_{bcp} > 1$) in all cases. While covalent interactions are indicated by a $|V_{bcp}|/G_{bcp}$ ratio >2, interactions with pronounced ionic character are indicated by $|V_{bcp}|/G_{bcp} < 1$.[30] Thus, the ratio $|V_{bcp}|/G_{bcp}$ close to 1 found for the Pd–N and Pd–Cl bonds in **4a** and **6a** suggested increased ionicity. This finding was supported by the increased ratio of kinetic energy density to electron density (G_{bcp}/ρ_{bcp}) at the corresponding bond critical points. In contrast, the parameters determined for the Pd–C and Pd–P bonds, together with the more negative ratios of the total energy density to electron density, H_{bcp}/ρ_{bcp}, pointed to higher covalency.

The conversion of **4a** into **6a** was manifested mainly by greater electron density depletion at the bond critical points (as expressed by the Laplacian of electron density). The bond critical points for the Pd–C bonds in both complexes were close to the nodal surface in the Laplacian distribution (Fig. 5). In such cases, the profile of the Laplacian along the whole bond path could provide useful information.[31] Indeed, a comparison of the Laplacian profiles along the Pd–C bond path plotted against the normalised bond distance (Fig. 6) showed that carbene formation was associated not only with electron density depletion at the bond critical point but also with a significant charge accumulation in the region of the carbene lone electron pair.

Electrochemistry

The redox properties of complexes **4–7** were studied by cyclic voltammetry on a glassy carbon disc electrode in dichloromethane containing $Bu_4N[PF_6]$ as the supporting electrolyte. The redox behaviour of the imidoyl complexes **4** and **5** was generally similar (Fig. 7 and S13,† data in Table 4). Initially,

Table 3 Values of electron density (ρ_{bcp}), Laplacian of the electron density ($\nabla^2\rho_{bcp}$), total electronic density (H_{bcp}), the ratio of potential and kinetic energy density ($|V_{bcp}|/G_{bcp}$), and the ratios of kinetic (G_{bcp}/ρ_{bcp}) and total energy density (H_{bcp}/ρ_{bcp}) to electron density at the bond critical point (bcp) located between the palladium and the coordinated donor atoms as well as the corresponding bond distances (experimental and calculated) and delocalisation indices (DI)

		Bond length [Å]								
Compound	Bond	Exp.	Calc.[a]	ρ_{bcp} [e Å^{-3}]	$\nabla^2\rho_{bcp}$ [e Å^{-5}]	H_{bcp} [a.u.]	$\lvert V_{bcp}\rvert/G_{bcp}$ [a.u.]	G_{bcp}/ρ_{bcp} [a.u.]	H_{bcp}/ρ_{bcp} [a.u.]	DI
4a	Pd–C	1.986	2.000	0.139	0.150	−0.065	1.64	0.73	−0.47	0.894
	Pd–P	2.266	2.273	0.108	0.112	−0.045	1.62	0.68	−0.42	0.890
	Pd–N	2.201	2.248	0.071	0.247	−0.012	1.16	1.04	−0.17	0.463
	Pd–Cl	2.416	2.445	0.065	0.195	−0.013	1.21	0.94	−0.2	0.613
6a	Pd–C	1.978	1.978	0.142	0.260	−0.065	1.50	0.92	−0.46	0.925
	Pd–P	2.273	2.291	0.107	0.081	−0.044	1.68	0.61	−0.41	0.871
	Pd–N	2.187	2.240	0.073	0.244	−0.013	1.18	1.01	−0.18	0.482
	Pd–Cl	2.363	2.358	0.079	0.219	−0.019	1.27	0.94	−0.24	0.733

[a] Calculated at the B3LYP(d3bj)/def2-TZVPP:sdd(Pd); a.u. = atomic units.

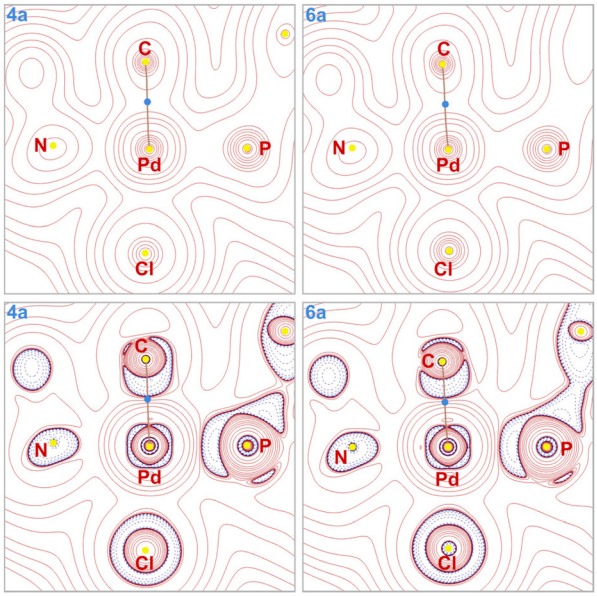

Fig. 5 (top) Contour plots of the electron density ρ in the plane defined by P, Pd and C atoms and (bottom) Laplacian contours ($\nabla^2\rho$; positive – full red lines, negative – dashed blue lines) for **4a** and **6a** (atomic critical points are shown yellow circles, bond critical points as blue circles, and bond paths corresponding to the Pd–C bonds as brown lines).

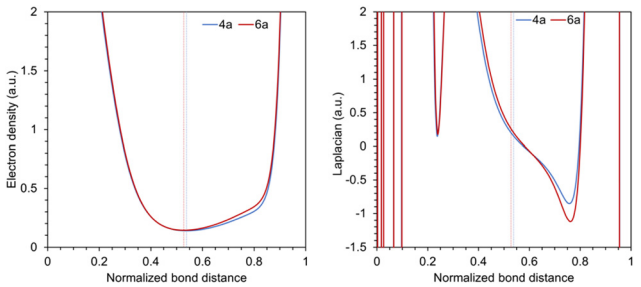

Fig. 6 Plots of electron density (ρ, left) and its Laplacian ($\nabla^2\rho$, right) along the normalised bond length of the Pd–C bond in **4a** (blue line) and **6a** (red line). Weak vertical lines represent the locations of the bond critical points.

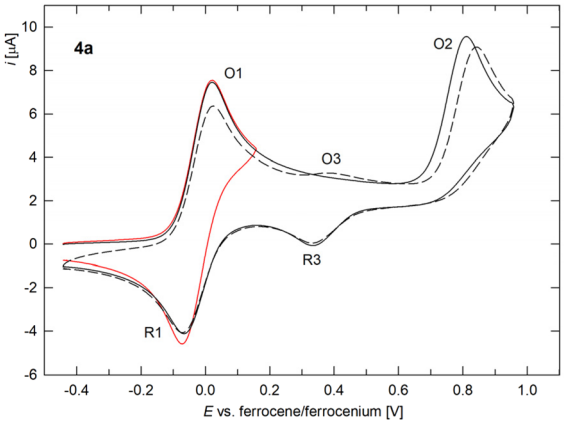

Fig. 7 Cyclic voltammograms of **4a** recorded at a glassy carbon electrode in dichloromethane containing $Bu_4N[PF_6]$ as the supporting electrolyte and a 100 mV s^{-1} scan rate. The second scan is shown by a dashed line.

Table 4 Summary of the electrochemical data[a]

Compound	Ferrocene oxidation E° (O1/R1)	Additional processes
4a	−0.03	$E_{pa}(O2) \approx 0.9$, $E_{pc}(R3) \approx 0.35$
4b	0.00	$E_{pa}(O2) \approx 0.8$, $E_{pc}(R3) \approx 0.39$
5a	0.00	$E_{pa}(O2) \approx 0.9$, $E_{pc}(R3) \approx 0.34$
5b	0.01	$E_{pa}(O2) \approx 0.9$, $E_{pc}(R3) \approx 0.37$
6a	0.43	$E_{pc}(R2) = -1.68$
6b	0.46	$E_{pc}(R2) = -1.89$
7a	0.44	$E_{pc}(R2) = -1.59$
7b	0.46	$E_{pc}(R2) = -1.79$

[a] The potentials are given in volts relative to the ferrocene/ferrocenium reference (for details, see Experimental). The potentials for the reversible redox processes were determined as the average of the anodic (E_{pa}) and cathodic (E_{pc}) peak potentials, $E^{\circ\prime} = \frac{1}{2}(E_{pa} + E_{pc})$. The peaks in the cyclic voltammograms were separated by 90–100 mV due to the large resistance. The decamethylferrocene standard showed similar values.

the compounds underwent reversible redox changes (O1/R1) at approximately 0 V *vs.* the ferrocene/ferrocenium reference,[32] which is significantly less than for FcNC itself ($E^{\circ\prime} \approx 0.30$ V in MeCN/$Bu_4N[BF_4]$).[11a] This redox process, which was negligibly affected by the nature of the chelating ligand L^{CY} and the phosphine, was attributed to one-electron oxidation of the ferrocenyl group. Such assignment was supported by DFT calculations, which showed that the HOMO of the model compound **4a** was localised predominantly on the ferrocene unit (Fig. 8). An analysis of the frontier molecular orbitals using natural atomic orbitals (NAO) showed that the HOMO involved bonding overlap of the iron 3d orbitals (≈75%) with the π-systems of the cyclopentadienyl rings (≈10%, 2p of C). In contrast, the LUMO exhibited a high degree of delocalisation and was spanned across palladium (≈21%, 4d, 5s and 5p) and the donor atoms, including the carbene carbon (≈12%, 2s and 2p of C), phosphorus (≈8%, 3s and 3p of P), amine nitrogen (≈5%, 2s and 2p of N) and chloride (≈3%, 3s and 3p).

At higher potentials, compounds **4** and **5** displayed an additional, ill-defined irreversible oxidation (O2) peak at approximately 0.8–0.9 V. The oxidative wave was associated with a weak cathodic counterwave (R3) during the reverse scan, and upon repeated scanning, a weak oxidative wave (O3) was detected (hardly discernible for some compounds), most likely associated with the cathodic event R3. The waves R3 and O3 were attributed to electrochemically generated species. Overall, this suggested that the second oxidation was followed by chemical steps that produced another redox-active species (ECE mechanism). For PMe_3 complexes **4b** and **5b**, the second wave was composite, followed by a more or less separated post-wave, and for compound **5b**, two weak reduction waves were observed and attributed to the generated species. Notably, no defined waves were detected in the cathodic region for **4** and **5**. Typically, several weak reduction waves were observed, attribu-

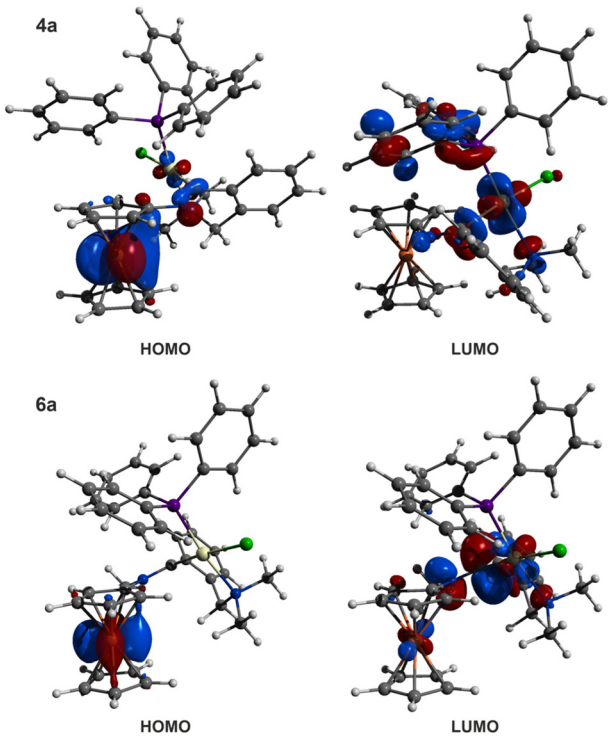

Fig. 8 Frontier orbitals of **4a** and the cation in **6a** (isosurfaces at ±0.05 a.u. are shown).

table to electrochemically generated and/or decomposition products (see ESI†).

In the accessible potential range, the carbene complexes **6** and **7** displayed one reversible redox change (waves O1 and R1) and one irreversible, probably two-electron reduction (R2; Fig. 9 and S14,† Table 4). The chemical reactions associated with reduction R1 (*e.g.*, decomposition of the electrogenerated species) produced additional redox-active species, which were oxidised during the following scans, giving rise to weak, broad waves at potentials lower than those for O1. Notably, the voltammogram shown in Fig. 9 did not change when the scan direction was reversed (*i.e.*, when the cathodic region was scanned first). However, the weak peak(s) due to the additional species were only observed after traversing the reduction wave R2.

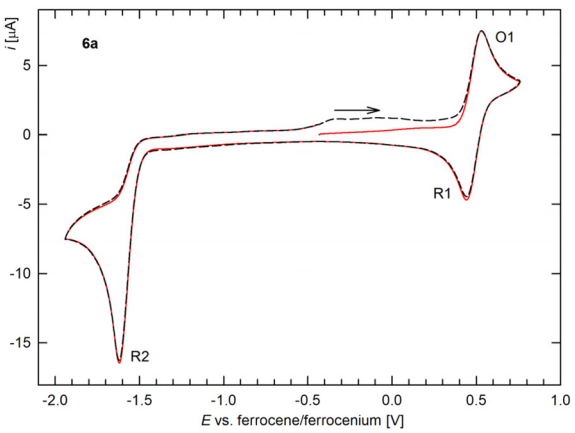

Fig. 9 Cyclic voltammograms of **6a**, recorded at a glassy carbon electrode in dichloromethane containing $Bu_4N[PF_6]$ as the supporting electrolyte and a 100 mV s^{-1} scan rate. The first and second scan are as a red solid line and a black dashed line, respectively; the initial scan direction is indicated with an arrow.

For the PMe_3 complexes **6b** and **7b**, an additional irreversible oxidation wave was observed just before O1 (see ESI†). In addition, **6b** and **7b** showed further irreversible oxidations (R2 and R3) when the scan range was extended towards more negative potentials. No similar waves were observed for the analogous PPh_3 complexes.

Based on an inspection of the frontier orbitals (Fig. 8), oxidation O1 was also attributed to the ferrocene/ferrocenium couple. Even in this case, the HOMO of **6a** was localised almost exclusively on the ferrocene moiety (≈87%, 3d of Fe; ≈10%, 2p of C). The shift of the first oxidation towards more positive potentials (by approximately 0.4 V compared to the imidoyl complexes **4** and **5**) corresponded with the cationic nature of the carbene complexes, which made electron removal more difficult. Conversely, reduction R1 was strongly affected by the L^{CY} and phosphine ligands and was probably a Pd/carbene-centred redox process (likely a Pd(II)-to-Pd(0) reduction[33]). Indeed, the LUMO of **6a** was an anti-bonding orbital with major contributions from the carbon (≈43%, 2p) and nitrogen (≈10%, 2p) atoms of the carbene moiety, along with smaller admixtures of palladium (≈8%, 4d) and iron (≈5%, 3d) atoms.

Reactions of the imidoyl complexes with Brønsted and Lewis acids

The results of the IBO analysis suggesting the presence of a lone electron pair at the imidoyl nitrogen and previous reports describing the preparation of multinuclear complexes[34] and protic carbenes from imidoyl complexes[35] led us to further explore the reactivity of the representative complex **4a.**

Initially, we treated complex **4a** with *in situ*-generated (Ph_3P)-Au^+ in dichloromethane-methanol (Scheme 4). To our surprise, the reaction did not afford any Pd–Au complex but rather produced a burgundy red compound (see the UV-vis spectrum in Fig. 1), which was isolated in 52% yield by chromatography (23% after crystallisation) and structurally authenticated as (*Z*)-

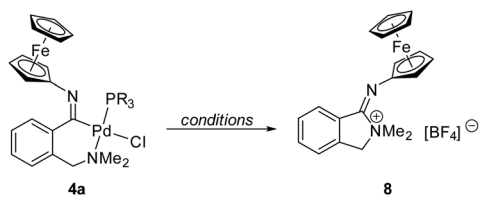

conditions	*yield of* ***8***
$[AuCl(PPh_3)]/Ag[BF_4]$ in CH_2Cl_2-MeOH	52%
$Ag[BF_4]$ in $CDCl_3$	70%
$NH_4[BF_4]$ in CH_2Cl_2-MeOH	26%

Scheme 4 Reaction of **4a** with Lewis and Brønsted acids to give **8**.

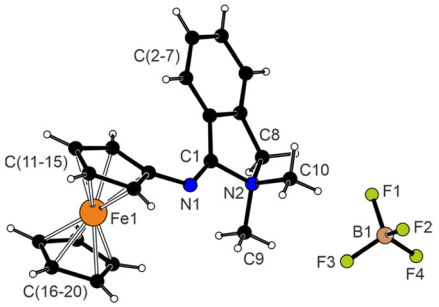

Fig. 10 Molecular structure of **8**. Selected distances and angles (in Å and deg): N1–C1 1.256(2), N1–C11 1.404(2), C1–N1–C11 123.2(1), N2–C1 1.530(2), N2–C8 1.518(2), N2–C9 1.496(2), N2–C10 1.506(2), C1–N2–C8 105.2(1) and C9–N2–C10 109.8(1); the carbon atoms forming the indolinium moiety, C(1–8), were coplanar to within 0.01 Å, and the N2 atom was displaced by 0.364(1) Å from this plane; the Fe1–C(11–15) bond lengths range 2.038(2)–2.055(2) Å, and the dihedral angle of the cyclopentadienyl planes was 2.5(1)°.

2,2-dimethyl-1-(ferrocenylimino)isoindolin-2-ium tetrafluoroborate (**8**) using spectroscopic methods and X-ray crystallography (Fig. 10). The addition of $Ag[BF_4]$ (1 equiv.) to **4a** in $CDCl_3$ led to a nearly 90% NMR yield of **8** (70% isolated yield at the 25 μmol scale). Attempts to similarly react complex **5a** ($Ag[BF_4]/CDCl_3$) were unsuccessful, most likely due to the different basicity of the sulfur atom in the SMe group replacing the NMe_2 moiety.

Subsequently, we treated **4a** with selected protic acids. While the addition of HCl (dioxane solution) to **4a** resulted in rapid decomposition, the reaction with $NH_4[BF_4]$ in dichloromethane-methanol again produced **8** in approximately 26% yield (based on NMR analysis; protic carbene analogous to **6a** was not detected). No reaction was observed with NH_4Cl and $K[BF_4]$, very likely due to the very limited solubilities of these salts and the absence of H^+ in the latter case.

The formation of **8** can be explained by reductive elimination[36] of the N,C-chelating imidoyl ligand from **4a**, presumably initiated by halide removal with an inorganic salt or Ag/Au reagents. The structure of **8** combining a quaternary nitrogen atom and an imine moiety is unique. While structurally related compounds, *e.g.*, aryl-$Cr(CO)_3$ complexes with oxopyrrolium ylide substituents, were previously obtained from thermally induced reactions of chromium aminocarbene complexes with alkynes,[37] the only similar compounds appear to be 2-oxoindolinium salts obtained by intramolecular cyclisation of 1-diazo-2-[2-(dialkylamino)phenyl]-2-oxoethylphosphonates proceeding *via* carbene intermediates[38,39] and 1-iminoisoindolines prepared in a conventional manner from 2-(chloromethyl)benzonitrile and amines.[40]

Conclusions

In summary, we demonstrated that Pd(II) complexes formed by orthopalladation of benzylic amines and thioethers and subsequent bridge cleavage with phosphines underwent facile insertion of isocyanoferrocene into their Pd–C bonds to provide structurally rigid, C,Y-chelating imidoyl complexes (Y = N, S) with pendant, redox-active ferrocenyl substituents. These imidoyl complexes were smoothly alkylated at the imine nitrogen with the Meerwein salt to provide the corresponding cationic aminocarbene complexes. Cyclic voltammetry supported by DFT calculations suggested that the primary oxidation of these compounds occurred at the peripheral ferrocene moiety. Furthermore, DFT calculations were used to rationalise the collected structural information. In particular, they showed that the imidoyl-to-carbene conversion represented the transformation of an X-type (σ-organyl) into an L-type (π-coordinated carbene) ligand. When attempting to synthesise protic carbene (analogous to **6a**) and heterometallic complexes from imidoyl complex **4a**, we noted that the compound rather underwent reductive elimination of the chelating imidoyl ligand, leading to 1-(ferrocenylimino)isoindolinium salt **8**.

Conflicts of interest

There are no conflicts of interest to declare.

Acknowledgements

This work was supported by the Charles University Research Centre Program (project no. UNCE/SCI/014) and by the Grant Agency of Charles University (project no. 222120). Computational resources were provided by the e-INFRA CZ project (ID 90254), supported by the Ministry of Education, Youth, and Sports of the Czech Republic.

References

1 R. Ramozzi, N. Chéron, B. Braïda, P. C. Hiberty and P. Fleurat-Lessard, *New J. Chem.*, 2012, **36**, 1137.
2 V. P. Boyarskiy, N. A. Bokach, K. V. Luzyanin and V. Y. Kukushkin, *Chem. Rev.*, 2015, **115**, 2698 and references cited therein.
3 L. Malatesta, in *Progr. Inorg. Chem*, ed. F. A. Cotton, Interscience Publishers, London, UK, 1959, vol. 1, pp. 283–379.
4 R. A. Michelin, A. J. L. Pombeiro and M. F. C. G. da Silva, *Coord. Chem. Rev.*, 2001, **218**, 75.
5 For reviews focused on carbene complexes, see: (*a*) F. E. Hahn and M. C. Jahnke, *Angew. Chem., Int. Ed.*, 2008, **47**, 3122; (*b*) P. de Frémont, N. Marion and S. P. Nolan, *Coord. Chem. Rev.*, 2009, **253**, 862; (*c*) M. N. Hopkinson, C. Richter, M. Schedler and F. Glorius, *Nature*, 2014, **510**, 485; (*d*) P. Bellotti, M. Koy, M. N. Hopkinson and F. Glorius, *Nat. Rev. Chem.*, 2021, **5**, 711.
6 For examples, see: (*a*) K. Hiraki, Y. Fuchita and T. Masumoto, *Bull. Chem. Soc. Jpn.*, 1980, **53**, 1171;

(*b*) D. L. Reger and J. E. Collins, *J. Organomet. Chem.*, 1995, **491**, 159.

7 K. Škoch, I. Císařová, J. Schulz, U. Siemeling and P. Štěpnička, *Dalton Trans.*, 2017, **46**, 10339.

8 (*a*) K. Škoch, I. Císařová, F. Uhlík and P. Štěpnička, *Dalton Trans.*, 2018, **47**, 16082; (*b*) K. Škoch, J. Schulz, I. Císařová and P. Štěpnička, *Organometallics*, 2019, **38**, 3060.

9 Complexes with C,N-ligands: (*a*) Y. Yamamoto and H. Yamazaki, *Inorg. Chim. Acta*, 1980, **41**, 229; (*b*) J. Dupont and M. Pfeffer, *J. Chem. Soc., Dalton Trans.*, 1990, 3193; (*c*) A. Zografidis, K. Polborn, W. Beck, B. A. Markies and G. van Koten, *Z. Naturforsch.*, 1994, **49**, 1494; (*d*) A. Böhm, K. Polborn, K. Sünkel and W. Beck, *Z. Naturforsch., B: J. Chem. Sci.*, 1998, **53**, 448; (*e*) J.-F. Ma, Y. Kojima and Y. Yamamoto, *J. Organomet. Chem.*, 2000, **616**, 149; (*f*) K.-E. Lee, H.-T. Jeon, S.-Y. Han, J. Ham, Y.-J. Kim and S. W. Lee, *Dalton Trans.*, 2009, 6578 Complexes with C,S-ligands: (*g*) J. Dupont, M. Pfeffer, J. C. Daran and Y. Jeannin, *Organometallics*, 1987, **6**, 899 For related systems, see: (*h*) L. Canovese, F. Visentin, C. Santo, C. Levi and A. Dolmella, *Organometallics*, 2007, **26**, 5590.

10 J. Dupont, C. S. Consorti and J. Spencer, *Chem. Rev.*, 2005, **105**, 2527.

11 (*a*) T. El-Shihi, F. Siglmüller, R. Herrmann, M. F. N. N. Carvalho and A. J. L. Pombeiro, *J. Organomet. Chem.*, 1987, **335**, 239; (*b*) G. R. Knox, P. L. Pauson, D. Willison, E. Solčániová and Š. Toma, *Organometallics*, 1990, **9**, 301.

12 For examples of studies focused on the coordination behaviour and reactivity of FcNC, see: (*a*) Y.-C. Huang, W.-Y. Lan, W.-M. Ching and S. C. N. Hsu, *New J. Chem.*, 2020, **44**, 18242; (*b*) M. V. Barybin, T. C. Holovics, S. F. Deplazes, G. H. Lushington, D. R. Powell and M. Toriyama, *J. Am. Chem. Soc.*, 2002, **124**, 13668; (*c*) V. N. Nemykin, A. A. Purchel, A. D. Spaeth and M. V. Barybin, *Inorg. Chem.*, 2013, **52**, 11004; (*d*) J. Mahrholdt, J. Noll, M. Korb, T. Rüffer and H. Lang, *Inorg. Chim. Acta*, 2022, **534**, 120829; (*e*) S. D. Waniek, C. Förster and K. Heinze, *Eur. J. Inorg. Chem.*, 2022, e202100905; (*f*) P. Vosáhlo, M. Franc, P. Harmach, J. Schulz and P. Štěpnička, *J. Organomet. Chem.*, 2023, **1000**, 122874.

13 For an overview of the chemistry of ferrocene-based carbenes, see: U. Siemeling, *Eur. J. Inorg. Chem.*, 2012, 3523.

14 For similar reactions involving $[(L^{CN})PdCl]_2$, see: (*a*) A. E. Kelly, S. A. Macgregor, A. C. Willis, J. H. Nelson and E. Wenger, *Inorg. Chim. Acta*, 2003, **352**, 79; (*b*) A. Mentes, R. D. W. Kemmitt, J. Fawcett and D. R. Russell, *J. Mol. Struct.*, 2004, **693**, 241.

15 D. C. D. Butler and C. J. Richards, *Organometallics*, 2002, **21**, 5433.

16 K. Nakamoto, *Infrared and Raman Spectra of Inorganic and Coordination Compounds, Part A: Theory and Applications in Inorganic Chemistry*, Wiley, Hoboken, NJ, 6th edn, 2009, ch. 2.6.1, pp. 192–204.

17 D. R. Scott and R. S. Becker, *J. Chem. Phys.*, 1961, **35**, 516.

18 (*a*) T. G. Appleton, H. C. Clark and L. E. Manzer, *Coord. Chem. Rev.*, 1973, **10**, 335; (*b*) F. R. Hartley, *Chem. Soc. Rev.*, 1973, **2**, 163.

19 B. Crociani, M. Sala, A. Polo and G. Bombieri, *Organometallics*, 1986, **5**, 1369.

20 G. R. Owen, R. Vilar, A. J. P. White and D. J. Williams, *Organometallics*, 2002, **21**, 4799.

21 K. Onitsuka, M. Yamamoto, S. Suzuki and S. Takahashi, *Organometallics*, 2002, **21**, 581.

22 For examples, see: (*a*) J. Silver, J. R. Miller, A. Houlton and M. T. Ahmet, *J. Chem. Soc., Dalton Trans.*, 1994, 3355; (*b*) V. Kovač, A. Višnjevac, V. Rapić and B. Kojić-Prodić, *J. Mol. Struct.*, 2004, **687**, 107; (*c*) W. Imhof, *Acta Crystallogr., Sect. E: Struct. Rep. Online*, 2009, **65**, m461.

23 (*a*) L. Lin, A. Berces and H.-B. Kraatz, *J. Organomet. Chem.*, 1998, **556**, 11; (*b*) L. Dufková, H. Matsumura, D. Nečas, P. Štěpnička, F. Uhlík and M. Kotora, *Collect. Czech. Chem. Commun.*, 2004, **69**, 351; (*c*) T. A. Fernandes, H. Solařová, I. Císařová, F. Uhlík, M. Štícha and P. Štěpnička, *Dalton Trans.*, 2015, **44**, 3092.

24 S. Fuertes, A. J. Chueca and V. Sicilia, *Inorg. Chem.*, 2015, **54**, 9885.

25 S. K. Schneider, P. Roembke, G. R. Julius, H. G. Raubenheimer and W. A. Herrmann, *Adv. Synth. Catal.*, 2006, **348**, 1862.

26 (*a*) G. Knizia, *J. Chem. Theor. Comput.*, 2013, **9**, 4834; (*b*) G. Knizia and J. E. M. N. Klein, *Angew. Chem., Int. Ed.*, 2015, **54**, 5518.

27 M. L. H. Green, *J. Organomet. Chem.*, 1995, **500**, 127.

28 (*a*) R. F. W. Bader, *Chem. Rev.*, 1991, **91**, 893; (*b*) R. F. W. Bader, *Acc. Chem. Res.*, 1985, **18**, 9.

29 (*a*) D. Cremer and E. Kraka, *Angew. Chem., Int. Ed. Engl.*, 1984, **23**, 627; (*b*) P. Macchi, D. M. Proserpio and A. Sironi, *J. Am. Chem. Soc.*, 1998, **120**, 13429; (*c*) P. Macchi and A. Sironi, *Coord. Chem. Rev.*, 2003, **238–239**, 383; (*d*) D. Stalke, *Chem. – Eur. J.*, 2011, **17**, 9264.

30 (*a*) R. Bianchi, G. Gervasio and D. Marabello, *Inorg. Chem.*, 2000, **39**, 2360; (*b*) E. Espinosa, I. Alkorta, J. Elguero and E. Molins, *J. Chem. Phys.*, 2002, **117**, 5529.

31 For examples, see: (*a*) M. W. Stanford, J. I. Schweizer, M. Menche, G. S. Nichol, M. C. Holthausen and M. J. Cowley, *Angew. Chem., Int. Ed.*, 2019, **58**, 1329; (*b*) A. Münch, L. Knauer, H. Ott, C. Sindlinger, R. Herbst-Irmer, C. Strohmann and D. Stalke, *J. Am. Chem. Soc.*, 2020, **142**, 15897; (*c*) B. Lindquist-Kleissler, J. S. Wenger and T. C. Johnstone, *Inorg. Chem.*, 2021, **60**, 1846.

32 G. Gritzner and J. Kůta, *Pure Appl. Chem.*, 1984, **56**, 461.

33 C. Amatore, M. Azzabi and A. Jutand, *J. Organomet. Chem.*, 1989, **363**, C41.

34 (*a*) T. Nakajima, M. Tsuji, N. Hamada, Y. Fukushima, B. Kure and T. Tanase, *J. Organomet. Chem.*, 2014, **768**, 61; (*b*) B. Crociani, R. Bertani, T. Boschi and G. Bandoli, *J. Chem. Soc., Dalton Trans.*, 1982, 1715; (*c*) R. Uson, J. Fornies, P. Espinet, E. Lalinde, P. G. Jones and G. M. Sheldrick, *J. Organomet. Chem.*, 1983, **253**, C47;

(*d*) M. Tanabiki, K. Tsuchiya, Y. Motoyama and H. Nagashima, *Chem. Commun.*, 2005, 3409.

35 D. L. Reger and J. E. Collins, *J. Organomet. Chem.*, 1995, **491**, 159.

36 (*a*) W. J. Marshall and V. V. Grushin, *Organometallics*, 2003, **22**, 1591; (*b*) A. C. Albéniz, P. Espinet, R. Manrique and A. Pérez-Mateo, *Chem. – Eur. J.*, 2005, **11**, 1565; (*c*) P. Veit, C. Förster and K. Heinze, *Beilstein J. Org. Chem.*, 2016, **12**, 1322.

37 (*a*) E. Chelain, R. Goumont, L. Hamon, A. Parlier, M. Rudler, H. Rudler, J.-C. Daran and J. Vaissermann, *J. Am. Chem. Soc.*, 1992, **114**, 8088; (*b*) E. Chelain, A. Parlier, M. Audouin, H. Rudler, J.-C. Daran and J. Vaissermann, *J. Am. Chem. Soc.*, 1993, **115**, 10568.

38 F. Léost, B. Chantegrel and C. Deshayes, *Tetrahedron Lett.*, 1997, **53**, 7557.

39 For the formation of 2-oxoindole derivatives by reductive elimination from Pd(II) complexes, see: R. Frutos-Pedreño, P. González-Herrero and J. Vicente, *Organometallics*, 2013, **32**, 4664.

40 F. S. Babichev and A. K. Tyltin, *Ukr. Khim. Zh.*, 1976, **36**, 62 and references therein.